

# VLTSeg: Simple Transfer of CLIP-Based Vision-Language Representations for Domain Generalized Semantic Segmentation

Christoph Hümmer<sup>1,3\*</sup>   Manuel Schwonberg<sup>1,3\*</sup>   Liangwei Zhou<sup>1,2\*</sup>  
 Hu Cao<sup>2</sup>   Alois Knoll<sup>2</sup>   Hanno Gottschalk<sup>3</sup>  
<sup>1</sup>CARIAD SE   <sup>2</sup>Technical University Munich   <sup>3</sup>Technical University Berlin  
 {manuel.schwonberg, christoph.huemmer}@cariad.technology  
 {liangwei.zhou, hu.cao, k}@tum.de  
 gottschalk@math.tu-berlin.de

## Abstract

Domain generalization (DG) remains a significant challenge for perception based on deep neural networks (DNN), where domain shifts occur due to lighting, weather, or geolocation changes. In this work, we propose VLTSeg to enhance domain generalization in semantic segmentation, where the network is solely trained on the source domain and evaluated on unseen target domains. Our method leverages the inherent semantic robustness of vision-language models. First, by substituting traditional vision-only backbones with pre-trained encoders from CLIP and EVA-CLIP as transfer learning setting we find that in the field of DG, vision-language pre-training significantly outperforms supervised and self-supervised vision pre-training. We thus propose a new vision-language approach for domain generalized segmentation, which improves the domain generalization SOTA by 7.6% mIoU when training on the synthetic GTA5 dataset. We further show the superior generalization capabilities of vision-language segmentation models by reaching 76.48% mIoU on the popular Cityscapes→ACDC benchmark, outperforming the previous SOTA approach by 6.9% mIoU on the test set at the time of writing. Additionally, our approach shows strong in-domain generalization capabilities indicated by 86.1% mIoU on the Cityscapes test set, resulting in a shared first place with the previous SOTA on the current leaderboard at the time of submission.

## 1. Introduction

In contrast to the recent advancements in computer vision due to deep learning [42, 63], domain shifts are still a major challenge for computer vision tasks. They can cause a significant performance decrease during inference time

\* indicates equal contribution

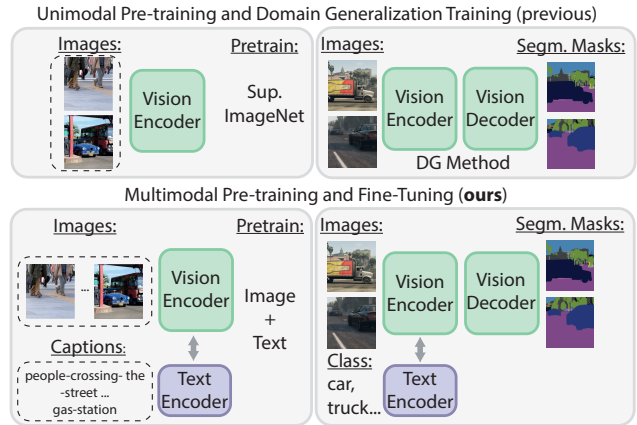


Figure 1. **CLIP-Based Fine-tuning for Domain Generalized Segmentation:** Previous works in domain generalization research mostly focus on applying methods (e.g. augmentations, consistency losses) in downstream training. We show that fine-tuning CLIP-based multimodal models that are pre-trained on image-text pairs significantly outperforms the current state-of-the-art in domain generalized semantic segmentation.

when the distribution differs from the training distribution [29, 80]. For this reason, two research fields have emerged to tackle domain shifts. Unsupervised domain adaptation (UDA) works with the assumption that unlabeled data from the target domain is available to adapt the network towards this particular domain. A large variety of methods have been developed in this field [28–30, 32, 69, 79, 80, 96, 97]. Nevertheless, unlabeled target data or information about the target domain(s) might not always be available during training time. In addition, data collection can be difficult, e.g. due to uncontrollable conditions like adverse weather situations or the sheer size of the operational domain. For this reason, the field of domain generalization (DG) developed to improve the generalization from only a single

(or multiple) source domain(s) to unseen target domains [12, 45, 53]. A variety of methods exists and several of them utilize domain randomization techniques in the input space [34, 45, 55, 68] or constrained feature representation learning [56].

Introduced by the foundational work of CLIP [59], vision-language models (VLMs) trained on large datasets of image-text pairs demonstrated remarkable generalization and zero-shot capabilities on a wide range of tasks, including segmentation [95]. In strong contrast to these findings, there are no existing approaches for domain generalized segmentation making use of the VLM capabilities.

For this reason, we investigate the potential of VLMs for domain generalization for semantic segmentation. Introducing both a straightforward transfer learning setting and a language-guided segmentation source training, we develop a simple yet competitive approach as described in Fig. 1 that takes advantage of the fact that text descriptions are largely domain-independent. We term this approach **VLT-Seg**, which describes our **V**ision-**L**anguage representation **T**ransfer for domain generalized **S**egmentation and employ vision-language models for the first time in this setting. Unlike previous DG approaches, VLT-Seg does not rely on or requires input-level augmentations [68, 75, 98, 100], consistency losses [45, 55, 92] or complex whitening losses in the feature space [12, 54, 56] but offers a simple and easily applicable method. The contribution of our work is, therefore, multi-folded:

- We utilize the CLIP and EVA-CLIP vision encoder weights for in a simple transfer learning setting and show that they provide a significantly better domain generalization performance than the vision-only pre-training and outperform the popular SegFormer [86] by 18.4% mIoU in average on three challenging real-world domains;
- We adapt the DenseCLIP [60] approach, employ a new, highly generalizing encoder initialization from EVA-CLIP [74] and employ Mask2Former [11] as the segmentation head. We improve the previous SOTA on the GTA5→Cityscapes benchmark by 7.6% abs. mIoU;
- VLT-Seg reaches a new SOTA domain generalization performance on Cityscapes→ACDC of 76.48% which exceeds the previous unsupervised SOTA performance by 6.93% mIoU. For in-domain generalization we reach 86.1% mIoU on the Cityscapes test set resulting in a shared first place with the previous best performing approach InternImage [84] on the official leaderboard of published approaches.

## 2. Related Work

### 2.1. Domain Generalization

Domain generalization (DG) approaches do not require any target data at all and only labeled source data and can be di-

vided into two major categories: distribution randomization and constrained feature learning. Our approach is the first one utilizing VLMs for domain generalization and related to constrained feature learning since the aligned multi-modal utilization of text and vision features works like a constraint in the embedding space.

To constrain the learning to domain invariant features, instance normalization and whitening techniques are commonly used [12, 53–55, 88] with different improvements like, e.g. semantic-aware whitening [56]. However, none of these methods included language-based constraints.

In domain randomization, the visual appearance of the input is modified to learn domain-invariant features. Several of these approaches use additional external real-world data like ImageNet for style randomization, often in combination with consistency losses [40, 45, 55, 92]. FSDR [34] differs by applying style randomization in the frequency space. WEDGE [39] samples real images from the internet and utilizes them and self-training.

In [68], the authors show that augmentations can already provide a state-of-the-art DG performance without external data. In contrast, both GBFA [75] and SHADE [98] employ feature-level augmentations. Recently, approaches tailored towards vision transformer architecture emerged in the field of DG, proposing enhanced attention mechanisms [3, 16, 73]. PromptFormer [22] was the first DG approach employing text prompts using an encoder from a diffusion model and proposing a scene and category prompt randomization strategy. This approach is related, but our method differs fundamentally in intuition, training strategy, and architecture. Our intuition is not to use generative pre-training but to directly use the supervision of text captions for semantic alignment of visual features. Moreover, we employ a simple loss function during our segmentation training, further promoting alignment.

### 2.2. Pre-Training and Generalization

Several works investigated the impact of supervised ImageNet pre-training on the downstream task [25, 36, 106] or up-scaling it to the larger 21k-ImageNet pre-training [62]. The generalization capabilities of ImageNet pre-training were also researched [19, 44, 89] showing that pre-training and downstream generalization not necessarily correlate.

In recent years, self-supervised image-based pre-training approaches have emerged. Earlier approaches [8, 23, 26] already showed a strong transferability to downstream tasks. More self-supervised pre-training methods were proposed in the following namely MoCov3 [9], DINO [6], DINOv2 [52], iBOT [102], masked image modeling (MIM) [87] and BEiTv2 [57] demonstrating highly generalizing and robust representations which transfer well to downstream tasks.

With the development of CLIP [59], supervised vision-

language pre-training showed strong zero-shot robustness, making it a promising candidate for pre-training. Consequently, several works building upon CLIP were proposed, such as EVA-CLIP [74] further improving, upscaling, and robustifying the vision-language pre-training.

### 2.3. Vision-Language Models

Vision Language Models (VLMs) combine vision and text features by training on large image-text pair datasets. A significant advantage of this training is the availability of image-text caption data, which can be extracted from the web and does not require manual labeling. That leads to massive datasets like the publicly available LAION-5B [67] dataset. The training methods can be divided into three main branches: The first implements contrastive learning by enforcing the similarity of corresponding text caption and image embeddings [38, 59, 70, 74, 103]. The second branch is about generative cost functions, for instance, masked image modeling and masked text modeling pre-training strategies [2, 20, 72, 83, 94], and the third branch introduces input modality adapters [1, 46, 58].

Several works adopted CLIP for tasks like object detection or semantic segmentation to profit from the classification capabilities and features. A straightforward extension is to apply CLIP to region-text pairs [71, 82, 99] to enable classification in object detection, especially of unlabeled objects. Similarly, semantic segmentation can be conducted based on CLIP by employing segment-text alignment [27, 47, 91, 105]. A simple approach for vision-language segmentation that provides architectural flexibility is DenseCLIP [60]. In this work, a vision and text are aligned on known classes during the segmentation training using an auxiliary loss.

## 3. Method

In this section, we will describe the general setting for our CLIP-based models and transfer learning setup. Moreover, we describe our VLTSeg method based on integrating the state-of-the-art decoder Mask2Former [11] and a simple loss function [60] that leads to dense vision-language alignment.

### 3.1. General Setting

An input image is defined as  $\mathbf{x}_n \in \mathbb{G}^{H \times W \times C}$  with  $\mathbb{G}$  being the integer color values,  $H$  and  $W$  height and width respectively and  $C$  denoting the number of channels. A deep segmentation network is defined as  $\mathbf{M}$  mapping the input images  $\mathbf{x}_n$  to output probability maps denoted as  $\mathbf{y}_n = (y_{n,i,s}) \in \mathbb{I}^{H \times W \times S}$ . They represent the class posterior probabilities  $y_{n,i,s} = P(s|i, \mathbf{x}_n)$  for each class  $s \in \mathcal{S}$  at pixel index  $i \in \mathcal{I} = \{1, 2, \dots, H \cdot W\}$  with  $\mathbb{I} = [0, 1]$ .

We furthermore define the encoder and decoder of a network  $\mathbf{M}$  as  $\mathbf{M}_E$  and  $\mathbf{M}_D$ , respectively. For the vision and language encoders we introduce the superscripts  $V$  and  $L$  respectively. We describe the vision encoder as  $\mathbf{M}_E^V$  and the language encoder as  $\mathbf{M}_E^L$ . Superscripts ‘‘S’’ and ‘‘T’’ on  $\mathbf{x}_n$  and  $\mathbf{y}_n$  denote the domain from which the variables stem, with e.g.,  $\mathcal{D}^S$  being the source domain and  $\mathcal{D}^T$  being the target domain. Since there are multiple possible unseen target domains in domain generalization, the target domains  $\mathcal{D}^{T_k}$  are indexed with  $k \in \mathcal{K} = \{1, 2, \dots, K\}$ . In domain generalization, we seek to train a model  $\mathbf{M}$  which generalizes well to these unseen target domains  $\mathcal{D}^{T_k}$ .  $\mathcal{T}$  denotes the space of text descriptions.

To motivate our approach mathematically, we consider the domain shift from  $\mathcal{D}^S$  to  $\mathcal{D}^T$  as a bijective map  $\mathcal{D}^S \ni \mathbf{x} \mapsto \phi(\mathbf{x}) \in \mathcal{D}^T$ . Note that learning such maps is a common computer vision task [101]. Let  $\mathcal{D}^S \cup \mathcal{D}^T \ni \mathbf{x} \mapsto T(\mathbf{x}) \in \mathcal{T}$  be the map which provides the text description to the image  $\mathbf{x}$ . We assume that, with high probability, the text description does not refer to the domain and thus remains valid in the new domain. E.g., if a scene in sunshine  $\mathbf{x}$  is transferred to the rainy domain by  $\phi(\mathbf{x})$ , the text description only changes if there is an explicit mention of weather in either of the scenes, which is assumed to be rare. Mathematically, this is expressed as  $T(\mathbf{x}) = T(\phi(\mathbf{x}))$  for  $\mathbf{x} \in \mathcal{D}^S$  with probability  $p \gg (1 - p) \geq 0$ . Furthermore, we assume perfect image-to-text feature alignment, i.e.  $\mathbf{M}_E^V(\mathbf{x}) = \mathbf{M}_E^L(T(\mathbf{x}))$  for  $\mathbf{x} \in \mathcal{D}^S \cup \mathcal{D}^T$ . Then we have:

**Lemma 1.** *Under the above assumptions, the encoder-decoder network  $\mathbf{M} = \mathbf{M}_D^V \circ \mathbf{M}_E^V$  is domain robust, i.e. provides the same output to  $\mathbf{x}$  and  $\phi(\mathbf{x})$ , with probability not smaller than  $p$ .*

*Proof.* With probability not less than  $p$ , we have for  $\mathbf{x} \in \mathcal{D}^S$

$$\mathbf{M}_E^V(\phi(\mathbf{x})) = \mathbf{M}_E^L(T(\phi(\mathbf{x}))) = \mathbf{M}_E^L(T(\mathbf{x})) = \mathbf{M}_E^V(\mathbf{x}).$$

Application of  $\mathbf{M}_D^V$  to both sides completes the proof.  $\square$

Our practical implementation of this idealized description builds upon large-scale vision-language pre-trainings as done by CLIP [59], or EVA-CLIP [18] with image-to-text feature alignment as a training objective. These produce highly generalizable encoder representations for  $\mathbf{M}_E^V$  and  $\mathbf{M}_E^L$ . Based on that, we propose to utilize these pre-trained encoders for our VLTSeg approach first in a simple, transfer learning-only setting and second within a novel vision-language learning framework for domain generalized segmentation. In the following, we will introduce the details of the two parts of our VLTSeg approach.

### 3.2. Transfer learning with CLIP-based vision encoder

In contrast to previous works, which employ complex auxiliary objectives or augmentations, we investigate to improve

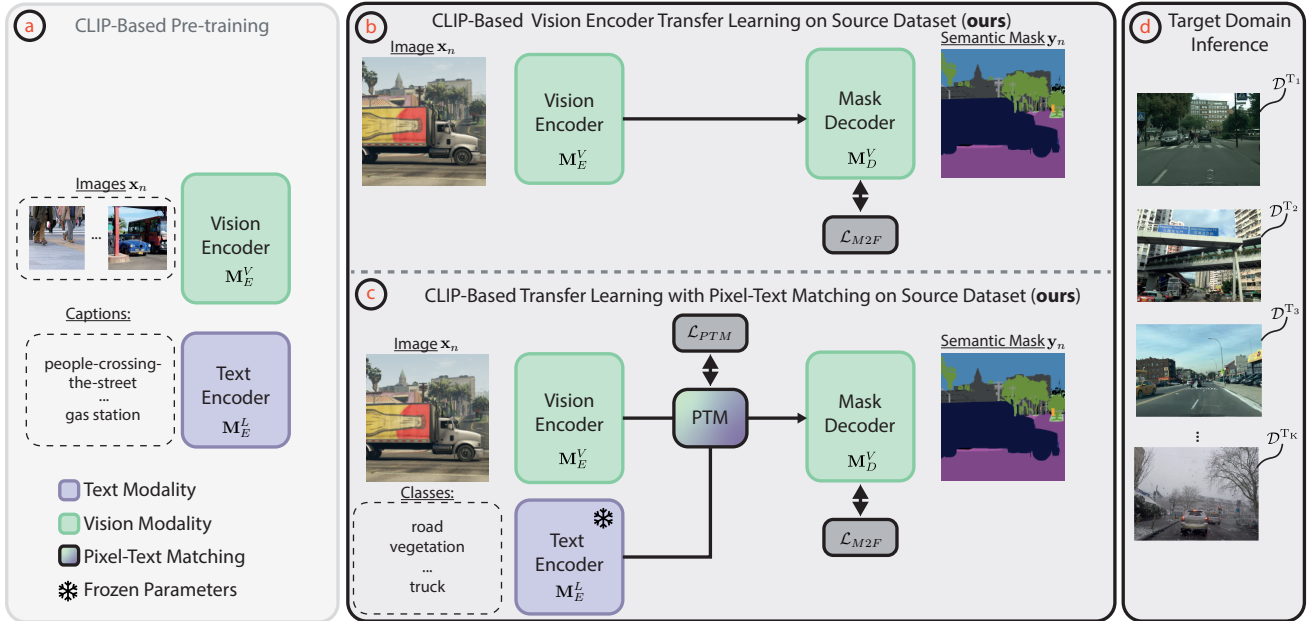


Figure 2. **Overall Framework of VLTSeg:** (a) contains the basis of our method, which is a vision-language pre-training to learn vision-language representations. The color green indicates the modality vision and the color purple the modality text. Here, we extract the pre-trained ViT and text encoder from either CLIP [59] or EVA-CLIP pre-training [74]. Afterwards, we employ either a fine-tuning in (b) with the vision encoder extracted from the pre-training stage. This encoder is fine-tuned with a Mask2Former [11] decoder on a source domain dataset. Alternatively, as a second method, we perform fine-tuning with the text and language encoder in described in (c) using an auxiliary loss and PTM alignment from [60] that retains vision-language alignment during fine-tuning. Ultimately, we analyze the transfer of the trained models to other target domains  $\mathcal{D}^{T_k}$  in (d).

domain generalization by fine-tuning. The straightforward way to employ pre-trained encoder weights for semantic segmentation is the utilization of a task-specific segmentation head and then fine-tuning the entire network  $\mathbf{M}$  on the downstream task, which is often done in computer vision [6, 52, 87, 102] and domain generalization [40, 45, 55, 92] with additional DG methods. For this reason, we designed a simple approach to fine-tune the vision encoder of a vision-language pre-training to investigate the zero-shot domain generalization from synthetic to unseen real domains. The encoder in our experiments  $M_E^V$  is initialized with either CLIP [59] or EVA-CLIP [18] pre-trained weights which are trained on image-text pairs as shown in Fig. 2 a.

We focus on transformer-based architectures ViT [17] and EVA [74] since they profit more from large-scale pre-training and a higher capacity than CNNs which benefits generalization, as shown previously by [21]. Moreover, we select the recently introduced transformer-based Mask2Former [11] as the decoder. This decoder based on mask classification was shown to be robust across multiple segmentation tasks and, therefore, fits well with our target objective of domain generalization. We decided to fully fine-tune the entire network  $\mathbf{M}$  as shown in Fig. 2 b since previous transfer learning works [33] have shown a

superior downstream performance when fully fine-tuning. Preliminary experiments confirmed these results. Specifically, in our transfer learning approach, we optimize the Mask2Former [11] loss function without modifications:

$$\mathcal{L}_{M2F} = \lambda_{CE}\mathcal{L}_{CE} + \lambda_{DICE}\mathcal{L}_{DICE} + \lambda_{BCE}\mathcal{L}_{BCE}, \quad (1)$$

where the masks are optimized by the binary cross entropy  $\mathcal{L}_{BCE}$  weighted by  $\lambda_{BCE}$  and the dice loss  $\mathcal{L}_{DICE}$  weighted by  $\lambda_{DICE}$ , the final classification loss  $\mathcal{L}_{CE}$  is weighted by  $\lambda_{CE}$ .

### 3.3. Vision-Language Guidance for Domain Generalization (VLTSeg)

In Sec. 3.2, we described a fine-tuning approach where we transferred only the visual representations and dropped the text encoder. In contrast, we now describe our entire VLT-Seg approach in detail, where we leverage the knowledge of the text embeddings during the downstream training to obtain generalized embeddings for the decoder.

We follow the design of the DenseCLIP [60] approach as a foundation for this method since it is tailored towards joint vision-language fine-tuning based on CLIP-initialized encoders. This method produces joint embeddings based on vision and language and optimizes the alignment of pixels

and text. A post-model prompting context decoder based on CoOp [104] processes learnable queries and representations from the vision encoder to generate a context embedding. Then, the features of the text encoder generated from dataset class prompts are updated with this context embedding. Ultimately, pixel-score maps are computed by a matrix multiplication between the text and vision encoder embeddings providing maps of the dimension  $r \in \mathbb{R}^{HW \times S}$  with  $S$  being the number of classes. We summarize all these steps with our PTM block in Fig. 2 c for simplicity. Since the classes are used as input prompts, an auxiliary loss function takes the score maps and ground truth as input:

$$\mathcal{L}_{\text{PTM}}^S = \frac{1}{N} \sum_{n=1}^N \sum_{k=1}^{H \times W} \sum_{c=1}^C y_{n,k,c}^S \log \left( \sigma \left( \frac{r_{n,k,c}^S}{\tau} \right) \right) \quad (2)$$

where  $\sigma$  denotes the softmax operation and  $\tau$  a temperature scaling. We propose two major novelties to the original DenseCLIP approach. First, we replace the FPN decoder that was used in DenseCLIP [60] with a Mask2Former [11] decoder proven to generalize well. Our second major change of the DenseCLIP framework is the choice of a new initialization for the vision encoder  $M_E^V$  and language encoder  $M_E^L$ . That is of high relevance since the weights of the language encoder remain frozen during training time, and we aim to utilize text embeddings for better generalization with our pixel-text matching guided VLTSeg approach. DenseCLIP originally initializes the encoder with weights from CLIP [59]. We argue that an initialization with a more sophisticated and even more large-scale pre-training than CLIP will further increase the domain generalization capabilities. For this reason, we propose to initialize both encoders with pre-trained weights from EVA-CLIP [18]. EVA-CLIP pre-trains on 2 billion text-image pairs (5-times of original CLIP), utilizes the LAMB optimizer and novel augmentations. EVA-CLIP shows significantly improved generalization capabilities.

Putting all together, we obtain the following final loss function for the downstream training of our VLTSeg approach:

$$\mathcal{L}_{\text{VLTSeg}} = \lambda_{\text{PTM}} \mathcal{L}_{\text{PTM}} + \mathcal{L}_{\text{M2F}}, \quad (3)$$

where  $\lambda_{\text{PTM}}$  denotes the loss weight for the auxiliary loss introduced by DenseCLIP. We do not modify the original DenseCLIP [60] loss. Also, note that VLTSeg is always trained on a single domain for all experiments, so it is either a labeled synthetic or real target domain. During the training time, none of the evaluation target domains is seen.

### 3.4. Relative Performance under Domain Shift

In domain adaptation and generalization the common evaluation metric is the mean intersection over union (mIoU). However, for the real-to-real domain shift evaluation (see Table 2) we would like to analyze the performance drop

from in- to out-of-domain performance.

For this reason we adapt the common robustness metric relative performance under corruption (rPC) [50] since corruptions are technically one form of domain shift. Based on their definition we propose our relative performance under domain shift (rPD) metric as:

$$\text{rPD} = \frac{\frac{1}{K} \sum_{k=1}^K \text{mIoU}^{\text{T}_k}}{\text{mIoU}^S} \quad (4)$$

The intuition behind the rPD is similar to the rPC. It measures the, over all target domain  $K$  averaged, relative performance drop caused by domain shift between the source domain with its clean oracle performance  $\text{mIoU}^S$  and the reduced performance  $\text{mIoU}^{\text{T}_k}$  on the unseen target domains  $\text{T}_k$ .

## 4. Experimental Settings

In the following, we introduce firstly the employed datasets and metrics. Afterwards, we introduce the network architectures and implementation details.

### 4.1. Datasets and Metrics

**Datasets:** According to the common domain generalization standard setting [22, 45, 56, 75, 85] we employ the two synthetic datasets SYNTHIA (SYN) [64] and GTA5 [61] as our source domains for our synthetic-to-real experiments. The datasets contain 9400 and 24966 images, respectively. We utilize Cityscapes [15], BDD100k [90], and Mapillary [51] as our real-world target domains with 500, 1000 and 2000 validation images, respectively. The training sets of these datasets remain unused in the synthetic-to-real experiments. As a common practice in domain generalization [39, 73, 93], we evaluate the experiments on the validation sets  $\mathcal{D}_{\text{val}}$  of the real-world target domain datasets and compute the domain generalization (DG) mean over Cityscapes, Mapillary and BDD. Compared to previous works, we extend the DG benchmark set of real-world datasets by the ACDC [65] dataset, which represents adverse weather conditions to also evaluate the generalization in this aspect.

**Metrics:** Next to our novel rPD metric, we follow common DG research practice for the evaluation metrics [35, 43, 77]. The mean intersection over union (mIoU) of  $S = 19$  segmentation classes [15, 61, 65] is used for the majority of experiments; only for SYNTHIA trainings only  $S = 16$  classes can be used. In addition, the mean of mIoUs on the target datasets is reported as DG mean.

### 4.2. Network Architectures

**Encoder** We utilize vision transformer (ViT)-based backbones [17] for all our experiments but with different initialization. Our default versions are the ViT-Large encoder with patch-size 14, and the EVA-02 [74] encoder, denoted

as ViT-L-14 and EVA-02-L-14 respectively. For our ablation studies also ViT-Base, denoted as ViT-B-16, is used. Note that we do not apply any own vision-language pre-training. For the synthetic-to-real experiments with a ResNet-backbone (see supplementary material), we also employed a ResNet-101 [24] encoder.

**Decoder Architecture** Our standard decoder architecture was the Mask2Former [11]. For ablation purposes, we also utilized the original DenseCLIP [60] FPN decoder [41], the ASPP-based DAFormer decoder [29] and the original SegFormer decoder [86]. All decoders were randomly initialized in our experiments.

### 4.3. Implementation Details

Our proposed method is implemented based on the open-source toolbox MMsegmentation [13] and MMDetection [7]. All experiments are conducted on  $2 \times$  A100 GPUs with 80GB each. For Mask2Former losses we employ  $\lambda_{CE} = 2.0$ ,  $\lambda_{BCE} = 5.0$  and  $\lambda_{DICE} = 5.0$  following the authors protocol [11]. We set  $\lambda_{PTM} = 1.0$  for the auxiliary loss. For a fair comparison with previous works, we used two different settings for the synthetic-to-real and real-to-real experiments. The synthetic-to-real experiments were conducted with a crop size of  $512 \times 512$  and a batch size 16. Only 5k fine-tuning iterations were necessary in this setting to avoid overfitting to the synthetic source domain. The real-to-real experiments used a larger crop size of  $1024 \times 1024$  and batch size 8 to better compare with HGFormer [16] and all trained on 20k iterations. For evaluation, we always select the last checkpoint of a training in line with previous works [37, 68].

We use the same augmentations for all experiments: random resizing, random cropping, horizontal flip and color jitter. As the optimizer, we employ AdamW [48] for all our experiments as it is a common standard for training vision transformer models [11, 29, 77] with a default learning rate of 0.0001, and the backbone learning rate is established at one-tenth of the default rate. A learning rate schedule with a warm-up and decay was employed for a better fine-tuning of the pre-trained initialization. More extensive implementations details are provided in the supplement.

## 5. Results

In the following we first show the synthetic-to-real and real-to-real performance. Then we show the transfer learning results and discuss our ablation studies.

### 5.1. Synthetic-to-real domain generalization

In Table 1, we compare our VLTseg approach to other state-of-the-art methods for both GTA5- and SYNTHIA-source training. We significantly outperform the previous best work HRDA [31] by a margin of 7.6% mIoU on the

Table 1. **Domain generalization performance** (mIoU (%)) state-of-the-art approaches. Training was performed on the synthetic GTA5 ( $\mathcal{D}^S = \mathcal{D}_{train}^{GTA5}$ ) and SYNTHIA ( $\mathcal{D}^S = \mathcal{D}_{train}^{SYN}$ ). Evaluation is performed on three real-world validation sets ( $\mathcal{D}^T = \mathcal{D}_{val}$ ). Prior work results are cited from the respective paper, only the values for works marked with \* are taken from [73].

	DG Method	mIoU (%) on			
		$\mathcal{D}_{val}^{CS}$	$\mathcal{D}_{val}^{BDD}$	$\mathcal{D}_{val}^{MV}$	DG mean
$\mathcal{D}^S$ : GTA5	Baseline [86]	46.6	45.6	50.1	47.4
	AdvStyle* [100]	46.6	45.1	48.4	46.7
	ReVT [77]	50.0	48.0	52.8	50.3
	DAFormer [29]	52.7	47.9	54.7	51.7
	SHADE* [98]	53.3	48.2	55.0	52.2
	PromptFormer [22]	52.0	-	-	-
	IBAFORMER [73]	56.3	49.8	58.3	54.8
	CMFormer [3]	55.3	49.9	60.1	55.1
	HRDA [31]	57.4	49.1	61.2	55.9
	VLTseg (Ours)	<b>65.6</b>	<b>58.4</b>	<b>66.5</b>	<b>63.5</b>
$\mathcal{D}^S$ : SYNTHIA	Baseline [86]	41.4	36.2	42.4	40.0
	ReVT [77]	46.3	40.3	44.8	43.8
	CMFormer [3]	44.6	33.4	43.3	40.4
	PromptFormer [22]	49.3	-	-	-
	IBAFORMER [73]	50.9	44.7	50.6	48.7
	VLTseg (Ours)	<b>56.8</b>	<b>50.5</b>	<b>54.5</b>	<b>53.9</b>

DG mean for GTA5 as source and 5.2% mIoU with SYNTHIA marking a large step for domain generalization performance. This shows the strong generalization capabilities of vision-language pre-training and language guidance since we do not employ any specialized loss functions as other approaches to enforce DG. We also conducted experiments with a ResNet-101 [24] backbone and reached SOTA performance (see supplement).

### 5.2. Real-to-real domain generalization

To extensively evaluate the domain generalization across the four real-world datasets, we designed a cross-correlation experiment as shown in Table 2.

We can observe that our VLTseg approach shows a significantly better domain generalization across all datasets, both in terms of absolute mIoU and our rPD metric. The gains are significant in comparison with the SegFormer architecture [86], which is commonly used in domain adaptation and generalization. When training on Cityscapes, VLTseg improves the rPD by +9% and by +13.7% mIoU on ACDC. Similarly, when training on Mapillary, we improve significantly on ACDC by +8.1% mIoU and by +3.5% on the rPD

Table 2. **Cross-wise real-to-real domain generalization performance** (mIoU (%)). Training was performed on the real-world dataset as shown row-wise. In- and out-of-domain performance evaluation was conducted on various real-world validation sets. The in-domain performance is marked with gray. Except the values from [16] experiments were conducted by ourselves.

Method		Evaluated on					rPD metric
		$\mathcal{D}_{val}^{CS}$	$\mathcal{D}_{val}^{BDD}$	$\mathcal{D}_{val}^{MV}$	$\mathcal{D}_{val}^{ACDC}$		
Train	$\mathcal{D}_{train}^{CS}$	SegFormer [86]	80.8	58.0	69.1	58.6	76.6
		SAM-ViT[42]+M2F	82.8	57.1	71.0	60.5	75.9
		HGFormer [16]	-	61.5	72.1	67.2	-
		VLTSeg (Ours)	<b>83.0</b>	<b>64.4</b>	<b>76.4</b>	<b>72.3</b>	<b>85.6</b>
	$\mathcal{D}_{train}^{BDD}$	SegFormer [86]	62.4	64.4	63.0	54.2	93.0
		SAM-ViT[42]+M2F	68.8	69.3	69.1	57.9	94.2
		VLTSeg(Ours)	<b>72.5</b>	<b>69.7</b>	<b>72.7</b>	<b>65.5</b>	<b>100.8</b>
	$\mathcal{D}_{train}^{MV}$	SegFormer [86]	76.1	63.0	78.9	65.7	86.5
		SAM-ViT[42]+M2F	76.4	62.8	78.9	63.4	85.6
		HGFormer [16]	78.2	66.3	-	-	-
		VLTSeg(Ours)	<b>80.2</b>	66.1	<b>81.5</b>	<b>73.8</b>	<b>90.0</b>
	$\mathcal{D}_{train}^{ACDC}$	SegFormer [86]	66.3	54.1	64.9	75.0	82.4
SAM-ViT[42]+M2F		68.9	57.0	68.1	77.4	83.5	
	VLTSeg (Ours)	<b>77.0</b>	<b>62.5</b>	<b>73.6</b>	<b>79.0</b>	<b>89.9</b>	

metric. Compared with the recent HGFormer [16], VLTSeg also mostly has a better real-to-real generalization. We additionally fine-tuned a ViT-backbone initialized with Segment Anything (SAM) [42] as it is the largest segmentation vision pre-training dataset currently available. The generalization performance of SAM pre-trained weights is dataset-dependent but overall not significantly higher than for the ImageNet pre-trained SegFormer [86]. Our approach reaches a significantly better generalization than SAM, which shows that VLTSeg performs superior over large-scale vision-only pre-training. As shown in table 3, our VLTSeg approach outperforms the previous domain adaptation SOTA significantly by +6.93% mIoU on the ACDC test set even though we are not using any ACDC samples during training. This performance translates into first place on the official leaderboard with a substantial margin by the time of writing. For the in-domain performance on  $\mathcal{D}_{test}^{CS}$ , we obtain 86.1% mIoU, marking the shared best performance with InternImage [84] on the official leaderboard. Note that this performance is achieved without an extended training dataset [5, 76, 84] or a huge model [84] showing the effectiveness of our approach.

### 5.3. Transfer Learning

Our transfer learning results for synthetic source datasets are shown in Table 4. It allows a comparison between the three different pre-training paradigms: ImageNet supervised pre-training, vision self-supervised pre-training, and

Table 3. **Test set Performance of our approach on Cityscapes and ACDC** in (mIoU (%)) compared with previous state-of-the-art methods. The detailed settings for these experiments can be found in the appendix. Rank denotes the position on the official Cityscapes leaderboard of published approaches.

Cityscapes ( $\mathcal{D}_{train}^{CS}$ ) $\rightarrow$ Cityscapes ( $\mathcal{D}_{test}^{CS}$ )				Cityscapes ( $\mathcal{D}_{train}^{CS}$ ) $\rightarrow$ ACDC ( $\mathcal{D}_{test}^{ACDC}$ )		
Method	Rank	Venue	mIoU in %	Method	UDA/DG	mIoU in %
ViT-Adapter-L [10]	4	ICLR2023	85.2	HRDA [30]	UDA	67.96
InverseForm [5]	2	CVPR2021	85.6	CISS [66]	UDA	69.55
HS3 [4]	3	BMVC2021	85.7	PromptFormer [22]	DG	62.0
InternImage [84]	1	CVPR2023	<b>86.1</b>	VLTSeg (Ours) (512 <sup>2</sup> )	DG	75.12
VLTSeg (Ours)	1		<b>86.1</b>	VLTSeg (Ours) (1024 <sup>2</sup> )	DG	<b>76.48</b>

vision-language pre-training.

First, we observe that the recent self-supervised vision pre-trained methods provide a stronger generalization than supervised pre-training since DEiT [78] outperforms supervised training by +5.7% mIoU. Surprisingly, SAM performs slightly worse than DEiT but still outperforms ImageNet supervised training. Similar to the real-to-real generalization, SAM is dataset-dependent and shows a weaker generalization than vision-language pre-training.

Notably, the CLIP [59] initialization performs even stronger on the DG mean than DEiT by +1.2% mIoU, indicating that vision-language pre-training strongly benefits from the larger datasets and the task-agnostic image-text pair training. When we employ the EVA-CLIP [74] initialization, we obtain a further increase of +8.2% mIoU over CLIP. Similar effects can be observed when training only on SYNTHIA. Vision-language pre-training datasets contain a multitude of samples compared to self-supervised vision datasets, e.g. SAM with 11 million images has only a fraction of the 2 billion image-text pairs used for EVA-CLIP [74] pre-training. We consider this an inherent advantage of vision-language pre-training since collecting these datasets is easier, and the dataset sizes are significantly larger [59].

### 5.4. Analysis

**Feature Space Analysis** As the first part of a detailed analysis of our approach, we perform a t-SNE-analysis [81] of our embedding space before and after training with our VLTSeg approach. The result is shown in Figure 8. We observe that after training with our VLTSeg approach solely on the synthetic GTA5 dataset, we observe significantly better aligned and, more importantly, overlapping clusters for both GTA5 and Cityscapes classes, confirming our initial hypothesis of a well-aligned feature space of vision-language models under domain shift.

**Encoder Ablation** Tab. 5 shows both the influence of model capacity and the downstream language guidance on the generalization performance. Nevertheless, note that all models are initialized with vision-language pre-trained weights.

First, independent from the language guidance, the larger the capacity of the architecture, the better the generalization. Between EVA-CLIP small and EVA-CLIP large, a

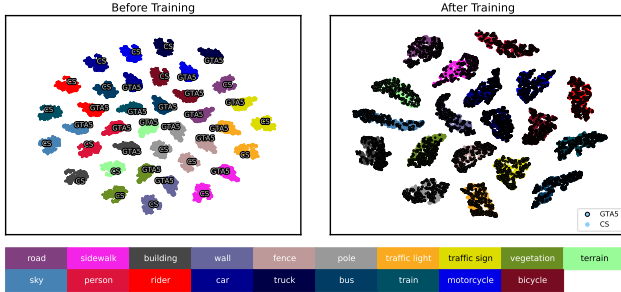


Figure 3. **t-SNE feature space analysis Cityscapes and GTA5 validation set.** We sampled 500 images from both  $\mathcal{D}_{\text{train}}^{\text{GTA5}}$  and  $\mathcal{D}_{\text{val}}^{\text{CS}}$  and process them with our best performing VLTseg network. We extract the embeddings after the text encoder, where both language and vision features are fused. On the right part, the GTA5 embeddings are denoted with black circles around their data points. From the plots, we can clearly see that synthetic source and real target class clusters are significantly better aligned and overlap after our VLTseg training. Best viewed digitally.

domain generalization improvement of +14.3% can be observed. The general improvement by the additional guidance from  $\mathcal{L}_{\text{PTM}}$  during the segmentation ranges for all models between 0.1%-2.3% depending on the model capacity, which is in line with the results from DenseCLIP [60]. More importantly, it can be observed that the effect of the language guidance on the generalization will decrease as the capacity of the vision encoder increases. With the EVA-CLIP initialization, the performance increase by language guidance is 2.3%, 1.4%, and 0.1% mIoU with increasing capacity from small to large, respectively. We reason that the vision encoder of the models with larger capacity already provides highly generalized embeddings.

Table 4. **Transfer Learning Domain Generalization Performance (mIoU (%))** of supervised source-only training on  $\mathcal{D}_{\text{train}}^{\text{GTA5}}$ . \* denotes that the ViT-L-16 was used as the encoder.  $\circ$  denotes that ViT-L-14 was used as the encoder. Mask2Former [11] was employed as the decoder for all experiments except for SegFormer.

		Pre-Training			mIoU in %					
		Method	Data	Sup.	Self-Sup.	$\mathcal{D}_{\text{val}}^{\text{CS}}$	$\mathcal{D}_{\text{val}}^{\text{BDD}}$	$\mathcal{D}_{\text{val}}^{\text{MV}}$	$\mathcal{D}_{\text{val}}^{\text{ACDC}}$	DG mean
$\mathcal{D}^{\text{S}}$ : GTA5	SV-SegFormer[86]	ImgNet-1K	✓	✗	46.6	45.6	50.1	36.4	44.7	
	Supervised*	ImgNet-21K	✓	✗	49.3	47.0	52.2	43.5	48.0	
	MoCov3*[9]	ImgNet-1K	✗	✓	49.7	46.2	52.4	39.1	46.9	
	DeiT3*[78]	ImgNet-21K	✓	✓	53.7	52.6	59.3	49.0	53.7	
	SAM*[42]	SA-1B	✓	✓	53.2	50.3	58.8	45.5	52.0	
	LDM [63]	LAION-5B	✓	✗	49.2	-	-	-	-	
	CLIP $\circ$ [59]	WIT	✓	✗	55.6	52.5	59.9	51.5	54.9	
EVA-02 $\circ$ [74]	Merged-2B	✓	✗	<b>65.3</b>	<b>58.3</b>	<b>66.0</b>	<b>62.6</b>	<b>63.1</b>		
$\mathcal{D}^{\text{S}}$ : SYNTHIA	SV-SegFormer[86]	ImgNet-1K	✓	✗	41.1	36.2	42.4	32.6	38.1	
	Supervised*	ImgNet-21K	✓	✗	44.3	37.1	43.1	34.8	39.8	
	MoCov3*[9]	ImgNet-1K	✗	✓	40.2	35.4	41.5	31.7	37.2	
	DeiT3*[78]	ImgNet-21K	✓	✓	47.8	39.1	45.4	34.7	41.8	
	SAM*[42]	SA-1B	✓	✓	51.6	40.4	50.1	40.1	45.6	
	CLIP $\circ$ [59]	WIT	✓	✗	51.1	44.7	50.6	40.7	46.8	
	EVA-02 $\circ$ [74]	Merged-2B	✓	✗	<b>56.8</b>	<b>51.9</b>	<b>55.1</b>	<b>48.5</b>	<b>53.1</b>	

Table 5. **Ablation study of different vision-language encoder initializations and complexities** and their domain generalization performance (mIoU (%)). Employed decoder was Mask2Former [11] Training was performed on the synthetic GTA5 ( $\mathcal{D}^{\text{S}} = \mathcal{D}_{\text{train}}^{\text{GTA5}}$ ) dataset. Evaluation is performed on four real-world datasets. \* denotes training over 20k iterations.

Init	Encoder	$\mathcal{L}_{\text{PTM}}$	mIoU in %				
			$\mathcal{D}_{\text{val}}^{\text{CS}}$	$\mathcal{D}_{\text{val}}^{\text{BDD}}$	$\mathcal{D}_{\text{val}}^{\text{MV}}$	$\mathcal{D}_{\text{val}}^{\text{ACDC}}$	DG mean
CLIP	ViT-B-16	✗	50.0	45.0	54.3	42.5	48.0
		✓	47.5	45.7	54.3	41.2	47.2
CLIP	ViT-L-14	✗	55.6	52.5	59.9	51.5	54.9
		✓	55.6	52.7	59.6	49.2	54.3
EVA-02*	EVA-02-S-16	✗	45.9	47.5	51.7	41.3	46.6
		✓	52.6	48.9	53.3	40.7	48.9
EVA-02	EVA-02-B-16	✗	54.9	50.3	57.2	46.6	52.3
		✓	54.5	52.9	59.5	47.9	53.7
EVA-02	EVA-02-L-14	✗	65.3	58.3	66.0	62.6	63.1
		✓	65.6	58.4	66.5	62.2	63.2

We provide more details like a loss hyperparameter ablation, our decoder ablation, qualitative examples, and an ablation for real-to-real transfer learning in the supplement.

## 5.5. Limitations

Our standard encoder is the EVA-02-L-14 with 304M parameters and therefore 3.7 $\times$  the parameters of the SegFormer-MiT-B5 encoder [86] which was used for several previous state-of-the-art works. Therefore, our approach requires more training resources in terms of GPU memory and time and is, similar to other DG approaches, not directly applicable to real-time settings.

## 6. Conclusion

In this work, we introduced a novel approach for an effective utilization of vision-language representations for domain generalized segmentation motivated by the observation that textual descriptions often do not explicitly refer to a domain and, therefore, tend to be domain invariant. By image-to-text feature alignment, vision features gradually inherit invariance and make image perception more robust against domain shifts.

By leveraging large-scale vision-language pre-training and language guidance during segmentation training, we outperformed previous state-of-the-art methods significantly and showcased the potential of VLMs for domain generalization. We also observed a superior performance on several real-to-real benchmarks for our approach, reaching a new state-of-the-art performance on ACDC with a large margin. Overall, our results further evolve the established strategy for domain generalization of initializing models with ImageNet pre-training to the utilization of vision-language pre-training and guidance.

## References

- [1] Jean-Baptiste Alayrac, Jeff Donahue, Pauline Luc, Antoine Miech, Iain Barr, Yana Hasson, Karel Lenc, Arthur Mensch, Katherine Millican, Malcolm Reynolds, Roman Ring, Eliza Rutherford, Serkan Cabi, Tengda Han, Zhitao Gong, Sina Samangooei, Marianne Monteiro, Jacob L Menick, Sebastian Borgeaud, Andy Brock, Aida Nematzadeh, Sahand Sharifzadeh, Miłkoł aj Bińkowski, Ricardo Barreira, Oriol Vinyals, Andrew Zisserman, and Karén Simonyan. Flamingo: a visual language model for few-shot learning. In *Proc. of NeurIPS*, 2022. 3
- [2] Hangbo Bao, Wenhui Wang, Li Dong, and Furu Wei. Vibeit: Generative vision-language pretraining, 2022. 3
- [3] Qi Bi, Shaodi You, and Theo Gevers. Learning Content-enhanced Mask Transformer for Domain Generalized Urban-Scene Segmentation. *arXiv:2307.00371*, pages 1–18, 2023. 2
- [4] Shubhankar Borse, Hong Cai, Yizhe Zhang, and Fatih Porikli. Hs3: Learning with proper task complexity in hierarchically supervised semantic segmentation. *arXiv preprint arXiv:2111.02333*, 2021. 7, 3
- [5] Shubhankar Borse, Ying Wang, Yizhe Zhang, and Fatih Porikli. Inverseform: A loss function for structured boundary-aware segmentation. In *Proc. of CVPR*, pages 5901–5911, 2021. 7, 3
- [6] Mathilde Caron, Hugo Touvron, Ishan Misra, Hervé Jégou, Julien Mairal, Piotr Bojanowski, and Armand Joulin. Emerging properties in self-supervised vision transformers. In *Proc. of ICCV*, pages 9650–9660, 2021. 2, 4
- [7] Kai Chen, Jiaqi Wang, Jiangmiao Pang, Yuhang Cao, Yu Xiong, Xiaoxiao Li, Shuyang Sun, Wansen Feng, Ziwei Liu, Jiarui Xu, et al. Mmdetection: Open mmlab detection toolbox and benchmark. *arXiv preprint arXiv:1906.07155*, 2019. 6
- [8] Ting Chen, Simon Kornblith, Mohammad Norouzi, and Geoffrey Hinton. A simple framework for contrastive learning of visual representations. In *Proc. of ICML*, pages 1597–1607. PMLR, 2020. 2
- [9] X Chen, S Xie, and K He. An empirical study of training self-supervised vision transformers. in 2021 ieee. In *Proc. of ICCV*, pages 9620–9629. 2
- [10] Zhe Chen, Yuchen Duan, Wenhai Wang, Junjun He, Tong Lu, Jifeng Dai, and Yu Qiao. Vision transformer adapter for dense predictions. *arXiv preprint arXiv:2205.08534*, 2022. 7
- [11] Bowen Cheng, Ishan Misra, Alexander G Schwing, Alexander Kirillov, and Rohit Girdhar. Masked-attention mask transformer for universal image segmentation. In *Proc. of CVPR*, pages 1290–1299, 2022. 2, 3, 4, 5, 6, 8, 1
- [12] Sungha Choi, Sanghun Jung, Huiwon Yun, Joanne T. Kim, Seungryoung Kim, and Jaegul Choo. RobustNet: Improving Domain Generalization in Urban-Scene Segmentation via Instance Selective Whitening. In *Proc. of CVPR*, pages 11580–11590, 2021. 2
- [13] MMsegmentation Contributors. Mmsegmentation: Openmmlab semantic segmentation toolbox and benchmark, 2020. 6
- [14] MMPreTrain Contributors. Openmmlab’s pre-training toolbox and benchmark. <https://github.com/openmmlab/mmpretrain>, 2023. 3
- [15] Marius Cordts, Mohamed Omran, Sebastian Ramos, Timo Rehfeld, Markus Enzweiler, Rodrigo Benenson, Uwe Franke, Stefan Roth, and Bernt Schiele. The cityscapes dataset for semantic urban scene understanding, 2016. 5, 3
- [16] Jian Ding, Nan Xue, Gui-Song Xia, Bernt Schiele, and Dengxin Dai. Hgformer: Hierarchical grouping transformer for domain generalized semantic segmentation. In *Proc. of CVPR*, pages 15413–15423, 2023. 2, 6, 7
- [17] Alexey Dosovitskiy, Lucas Beyer, Alexander Kolesnikov, Dirk Weissenborn, Xiaohua Zhai, Thomas Unterthiner, Mostafa Dehghani, Matthias Minderer, Georg Heigold, Sylvain Gelly, Jakob Uszkoreit, and Neil Houlsby. An Image is Worth 16x16 Words: Transformers for Image Recognition at Scale. In *Proc. of ICLR*, pages 1–21, 2021. 4, 5
- [18] Yuxin Fang, Quan Sun, Xinggang Wang, Tiejun Huang, Xinlong Wang, and Yue Cao. Eva-02: A visual representation for neon genesis. *arXiv preprint arXiv:2303.11331*, 2023. 3, 4, 5
- [19] Yutong Feng, Jianwen Jiang, Mingqian Tang, Rong Jin, and Yue Gao. Rethinking supervised pre-training for better downstream transferring. In *Proc. of ICLR*, 2021. 2
- [20] Xinyang Geng, Hao Liu, Lisa Lee, Dale Schuurmans, Sergey Levine, and Pieter Abbeel. Multimodal masked autoencoders learn transferable representations, 2022. 3
- [21] Micah Goldblum, Hossein Souri, Renkun Ni, Manli Shu, Viraj Uday Prabhu, Gowthami Somepalli, Prithvijit Chattopadhyay, Mark Ibrahim, Adrien Bardes, Judy Hoffman, Rama Chellappa, Andrew Gordon Wilson, and Tom Goldstein. Battle of the backbones: A large-scale comparison of pretrained models across computer vision tasks. In *Proc. of NeurIPS Datasets and Benchmarks Track*, 2023. 4
- [22] Rui Gong, Martin Danelljan, Han Sun, Julio Delgado Mangas, and Luc Van Gool. Prompting Diffusion Representations for Cross-Domain Semantic Segmentation. *arXiv:2307.02138*, pages 1–17, 2023. 2, 5, 7
- [23] Jean-Bastien Grill, Florian Strub, Florent Altché, Corentin Tallec, Pierre Richemond, Elena Buchatskaya, Carl Doersch, Bernardo Avila Pires, Zhaohan Guo, Mohammad Gheshlaghi Azar, et al. Bootstrap your own latent—a new approach to self-supervised learning. In *Proc. of NeurIPS*, 33:21271–21284, 2020. 2
- [24] Kaiming He, Xiangyu Zhang, Shaoqing Ren, and Jian Sun. Deep residual learning for image recognition. In *Proc. of CVPR*, pages 770–778, 2016. 6, 1
- [25] Kaiming He, Ross Girshick, and Piotr Dollár. Rethinking imagenet pre-training. In *Proc. of ICCV*, pages 4918–4927, 2019. 2
- [26] Kaiming He, Haoqi Fan, Yuxin Wu, Saining Xie, and Ross Girshick. Momentum contrast for unsupervised visual representation learning. In *Proc. of CVPR*, pages 9729–9738, 2020. 2
- [27] Wenbin He, Suphanut Jamonnak, Liang Gou, and Liu Ren. Clip-s4: Language-guided self-supervised semantic seg-

- mentation. In *Proc. of CVPR*, pages 11207–11216, 2023. 3
- [28] Judy Hoffman, Eric Tzeng, Taesung Park, Jun-Yan Zhu, Philip Isola, Kate Saenko, Alexei A. Efros, and Trevor Darrell. CyCADA: Cycle-Consistent Adversarial Domain Adaptation. In *Proc. of ICML*, pages 1989–1998, 2018. 1
- [29] Lukas Hoyer, Dengxin Dai, and Luc Van Gool. DAFormer: Improving Network Architectures and Training Strategies for Domain-Adaptive Semantic Segmentation. In *Proc. of CVPR*, pages 9924–9935, 2022. 1, 6
- [30] Lukas Hoyer, Dengxin Dai, and Luc Van Gool. HRDA: Context-Aware High-Resolution Domain-Adaptive Semantic Segmentation. In *Proc. of ECCV*, pages 372–391, 2022. 1, 7
- [31] Lukas Hoyer, Dengxin Dai, and Luc Van Gool. Domain Adaptive and Generalizable Network Architectures and Training Strategies for Semantic Image Segmentation. *arXiv:2304.13615*, pages 1–15, 2023. 6
- [32] Lukas Hoyer, Dengxin Dai, Haoran Wang, and Luc Van Gool. MIC: Masked Image Consistency for Context-Enhanced Domain Adaptation. In *Proc. of CVPR*, pages 11721–11732, 2023. 1
- [33] Jonathan Huang, Vivek Rathod, Chen Sun, Menglong Zhu, Anoop Korattikara, Alireza Fathi, Ian Fischer, Zbigniew Wojna, Yang Song, Sergio Guadarrama, et al. Speed/accuracy trade-offs for modern convolutional object detectors. In *Proc. of CVPR*, pages 7310–7311, 2017. 4
- [34] Jiaying Huang, Dayan Guan, Aoran Xiao, and Shijian Lu. FSDR: Frequency Space Domain Randomization for Domain Generalization. In *Proc. of CVPR*, pages 6891–6902, 2021. 2
- [35] Jiaying Huang, Dayan Guan, Aoran Xiao, and Shijian Lu. FSDR: Frequency space domain randomization for domain generalization. In *Proc. of CVPR*, pages 6891–6902, 2021. 5, 1
- [36] Minyoung Huh, Pulkit Agrawal, and Alexei A Efros. What makes imagenet good for transfer learning? *arXiv preprint arXiv:1608.08614*, 2016. 2
- [37] N. S. Jayant and P. Noll. *Digital Coding of Waveforms, Principles and Applications to Speech and Video*. Prentice Hall, 1984.
- [38] Chao Jia, Yinfei Yang, Ye Xia, Yi-Ting Chen, Zarana Parekh, Hieu Pham, Quoc Le, Yun-Hsuan Sung, Zhen Li, and Tom Duerig. Scaling up visual and vision-language representation learning with noisy text supervision. In *Proc. of ICML*, pages 4904–4916. PMLR, 2021. 3
- [39] Namyup Kim, Taeyoung Son, Cuiling Lan, Wenjun Zeng, and Suha Kwak. WEDGE: Web-Image Assisted Domain Generalization for Semantic Segmentation. *arXiv:2109.14196*, pages 1–14, 2021. 2, 5, 1
- [40] Sunghwan Kim, Dae-hwan Kim, and Hoseong Kim. Texture learning domain randomization for domain generalized segmentation. *arXiv preprint arXiv:2303.11546*, 2023. 2, 4
- [41] Alexander Kirillov, Ross Girshick, Kaiming He, and Piotr Dollár. Panoptic feature pyramid networks. In *Proc. of CVPR*, pages 6399–6408, 2019. 6
- [42] Alexander Kirillov, Eric Mintun, Nikhila Ravi, Hanzi Mao, Chloe Rolland, Laura Gustafson, Tete Xiao, Spencer Whitehead, Alexander C Berg, Wan-Yen Lo, et al. Segment anything. *arXiv preprint arXiv:2304.02643*, 2023. 1, 7
- [43] Marvin Klingner, Jan-Aike Termöhlen, Jacob Ritterbach, and Tim Fingscheidt. Unsupervised batchnorm adaptation (ubna): A domain adaptation method for semantic segmentation without using source domain representations. In *Proc. of WACV*, pages 210–220, 2022. 5
- [44] Simon Kornblith, Jonathon Shlens, and Quoc V Le. Do better imagenet models transfer better? In *Proc. of CVPR*, pages 2661–2671, 2019. 2
- [45] Suhyeon Lee, Hongje Seong, Seongwon Lee, and Euntae Kim. WildNet: Learning Domain Generalized Semantic Segmentation from the Wild. In *Proc. of CVPR*, pages 9936–9946, 2022. 2, 4, 5
- [46] Bo Li, Yuanhan Zhang, Liangyu Chen, Jinghao Wang, Jingkang Yang, and Ziwei Liu. Otter: A multi-modal model with in-context instruction tuning. *arXiv preprint arXiv:2305.03726*, 2023. 3
- [47] Feng Liang, Bichen Wu, Xiaoliang Dai, Kunpeng Li, Yinan Zhao, Hang Zhang, Peizhao Zhang, Peter Vajda, and Diana Marculescu. Open-vocabulary semantic segmentation with mask-adapted clip. In *Proc. of CVPR*, pages 7061–7070, 2023. 3
- [48] Ilya Loshchilov and Frank Hutter. Decoupled weight decay regularization. In *Proc. of ICLR*, 2018. 6
- [49] Leland McInnes, John Healy, and James Melville. Umap: Uniform manifold approximation and projection for dimension reduction. *arXiv preprint arXiv:1802.03426*, 2018. 3
- [50] Claudio Michaelis, Benjamin Mitzkus, Robert Geirhos, Evgenia Rusak, Oliver Bringmann, Alexander S Ecker, Matthias Bethge, and Wieland Brendel. Benchmarking robustness in object detection: Autonomous driving when winter is coming. *arXiv preprint arXiv:1907.07484*, 2019. 5
- [51] Gerhard Neuhold, Tobias Ollmann, Samuel Rota Buló, and Peter Kontschieder. The mapillary vistas dataset for semantic understanding of street scenes. In *Proc. of ICCV*, pages 4990–4999, 2017. 5, 4
- [52] Maxime Oquab, Timothée Darcet, Théo Moutakanni, Huy Vo, Marc Szafraniec, Vasil Khalidov, Pierre Fernandez, Daniel Haziza, Francisco Massa, Alaaeldin El-Nouby, et al. DINOv2: Learning robust visual features without supervision. *arXiv preprint arXiv:2304.07193*, 2023. 2, 4
- [53] Xingang Pan, Ping Luo, Jianping Shi, and Xiaoou Tang. Two at Once: Enhancing Learning and Generalization Capacities via IBN-Net. In *Proc. of ECCV*, pages 464–479, 2018. 2
- [54] Xingang Pan, Xiaohang Zhan, Jianping Shi, Xiaoou Tang, and Ping Luo. Switchable Whitening for Deep Representation Learning. In *Proc. of ICCV*, pages 1863–1871, 2019. 2
- [55] Duo Peng, Yinjie Lei, Lingqiao Liu, Pingping Zhang, and Jun Liu. Global and Local Texture Randomization for Synthetic-to-Real Semantic Segmentation. In *IEEE TIP*, 30:6594–6608, 2021. 2, 4

- [56] Duo Peng, Yinjie Lei, Munawar Hayat, Yulan Guo, and Wen Li. Semantic-Aware Domain Generalized Segmentation. In *Proc. of CVPR*, pages 2594–2605, 2022. 2, 5, 1
- [57] Zhiliang Peng, Li Dong, Hangbo Bao, Qixiang Ye, and Furu Wei. Beit v2: Masked image modeling with vector-quantized visual tokenizers. *arXiv preprint arXiv:2208.06366*, 2022. 2
- [58] Zhiliang Peng, Wenhui Wang, Li Dong, Yaru Hao, Shaohan Huang, Shuming Ma, and Furu Wei. Kosmos-2: Grounding multimodal large language models to the world. *ArXiv*, abs/2306, 2023. 3
- [59] Alec Radford, Jong Wook Kim, Chris Hallacy, Aditya Ramesh, Gabriel Goh, Sandhini Agarwal, Girish Sastry, Amanda Askell, Pamela Mishkin, Jack Clark, et al. Learning transferable visual models from natural language supervision. In *Proc. of ICML*, pages 8748–8763. PMLR, 2021. 2, 3, 4, 5, 7, 1
- [60] Yongming Rao, Wenliang Zhao, Guangyi Chen, Yansong Tang, Zheng Zhu, Guan Huang, Jie Zhou, and Jiwen Lu. Densenclip: Language-guided dense prediction with context-aware prompting. In *Proc. of CVPR*, pages 18082–18091, 2022. 2, 3, 4, 5, 6, 8, 1
- [61] Stephan R Richter, Vibhav Vineet, Stefan Roth, and Vladlen Koltun. Playing for data: Ground truth from computer games. In *Proc. of ECCV*, pages 102–118. Springer, 2016. 5, 4
- [62] Tal Ridnik, Emanuel Ben-Baruch, Asaf Noy, and Lihi Zelnik-Manor. Imagenet-21k pretraining for the masses. *arXiv preprint arXiv:2104.10972*, 2021. 2
- [63] Robin Rombach, Andreas Blattmann, Dominik Lorenz, Patrick Esser, and Björn Ommer. High-resolution image synthesis with latent diffusion models, 2021. 1
- [64] German Ros, Laura Sellart, Joanna Materzynska, David Vazquez, and Antonio M Lopez. The synthia dataset: A large collection of synthetic images for semantic segmentation of urban scenes. In *Proc. of CVPR*, pages 3234–3243, 2016. 5
- [65] Christos Sakaridis, Dengxin Dai, and Luc Van Gool. ACDC: The Adverse Conditions Dataset with Correspondences for Semantic Driving Scene Understanding. In *Proc. of ICCV*, pages 10765–10775, 2021. 5, 3, 4
- [66] Christos Sakaridis, David Bruggemann, Fisher Yu, and Luc Van Gool. Condition-invariant semantic segmentation. *arXiv preprint arXiv:2305.17349*, 2023. 7
- [67] Christoph Schuhmann, Romain Beaumont, Richard Vencu, Cade W Gordon, Ross Wightman, Mehdi Cherti, Theo Coombes, Aarush Katta, Clayton Mullis, Mitchell Wortsman, Patrick Schramowski, Srivatsa R Kundurthy, Katherine Crowson, Ludwig Schmidt, Robert Kaczmarczyk, and Jenia Jitsev. LAION-5b: An open large-scale dataset for training next generation image-text models. In *Proc. of NeurIPS Datasets and Benchmarks Track*, 2022. 3
- [68] Manuel Schwonberg, Fadoua El Bouazati, Nico M Schmidt, and Hanno Gottschalk. Augmentation-Based Domain Generalization for Semantic Segmentation. In *Proc. of IV - Workshops*, pages 1–8, 2023. 2, 6
- [69] Manuel Schwonberg, Joshua Niemeijer, Jan-Aike Termöhlen, Jörg P. Schäfer, Nico M. Schmidt, Hanno Gottschalk, and Tim Fingscheidt. Survey on Unsupervised Domain Adaptation for Semantic Segmentation for Visual Perception in Automated Driving. *IEEE Access*, 11:54296–54336, 2023. 1
- [70] Sheng Shen, Chunyuan Li, Xiaowei Hu, Yujia Xie, Jianwei Yang, Pengchuan Zhang, Anna Rohrbach, Zhe Gan, Lijuan Wang, Lu Yuan, et al. K-lite: Learning transferable visual models with external knowledge. In *Proc. of NeurIPS*, 2022. 3
- [71] Cheng Shi and Sibe Yang. Edadet: Open-vocabulary object detection using early dense alignment. In *Proc. of ICCV*, 2023. 3
- [72] Amanpreet Singh, Ronghang Hu, Vedanuj Goswami, Guillaume Couairon, Wojciech Galuba, Marcus Rohrbach, and Douwe Kiela. FLAVA: A foundational language and vision alignment model. In *Proc. of CVPR*, 2022. 3
- [73] Qiyu Sun, Huilin Chen, Meng Zheng, Ziyang Wu, Michael Felsberg, and Yang Tang. IBAFormer: Intra-batch Attention Transformer for Domain Generalized Semantic Segmentation. *arXiv:2309.06282*, pages 1–10, 2023. 2, 5, 6
- [74] Quan Sun, Yuxin Fang, Ledell Wu, Xinlong Wang, and Yue Cao. Eva-clip: Improved training techniques for clip at scale. *arXiv preprint arXiv:2303.15389*, 2023. 2, 3, 4, 5, 7, 1
- [75] Qiyu Sun, Pavlo Melnyk, Michael Felsberg, and Yang Tang. Augment Features Beyond Color for Domain Generalized Segmentation. *arXiv:2307.01703*, pages 1–10, 2023. 2, 5, 1
- [76] Andrew Tao, Karan Sapra, and Bryan Catanzaro. Hierarchical multi-scale attention for semantic segmentation. *arXiv preprint arXiv:2005.10821*, 2020. 7
- [77] Jan-Aike Termöhlen, Timo Bartels, and Tim Fingscheidt. A Re-Parameterized Vision Transformer (ReVT) for Domain-Generalized Semantic Segmentation. *arXiv:2308.13331*, pages 1–18, 2023. 5, 6
- [78] Hugo Touvron, Matthieu Cord, and Hervé Jégou. Deit iii: Revenge of the vit. In *Proc. of ECCV*, 2022. 7
- [79] Wilhelm Truhedden, Viktor Olsson, Juliano Pinto, and Lennart Svensson. DACS: Domain Adaptation via Cross-Domain Mixed Sampling. In *Proc. of WACV*, pages 1379–1389, 2021. 1
- [80] Yi-Hsuan Tsai, Wei-Chih Hung, Samuel Schulter, Kihyuk Sohn, Ming-Hsuan Yang, and Manmohan Chandraker. Learning to Adapt Structured Output Space for Semantic Segmentation. In *Proc. of CVPR*, pages 7472–7481, 2018. 1
- [81] Laurens Van der Maaten and Geoffrey Hinton. Visualizing data using t-sne. In *JMLR*, 9(11), 2008. 7
- [82] Tao Wang. Learning to detect and segment for open vocabulary object detection. In *Proc. of CVPR*, pages 7051–7060, 2023. 3
- [83] Wenhui Wang, Hangbo Bao, Li Dong, Johan Bjorck, Zhiliang Peng, Qiang Liu, Kriti Aggarwal, Owais Khan Mohammed, Saksham Singhal, Subhojit Som, and Furu Wei. Image as a foreign language: Beit pretraining for vision and vision-language tasks. In *Proc. of CVPR*, pages 19175–19186, 2023. 3

- [84] Wenhai Wang, Jifeng Dai, Zhe Chen, Zhenhang Huang, Zhiqi Li, Xizhou Zhu, Xiaowei Hu, Tong Lu, Lewei Lu, Hongsheng Li, et al. Internimage: Exploring large-scale vision foundation models with deformable convolutions. In *Proc. of CVPR*, pages 14408–14419, 2023. [2](#), [7](#), [3](#)
- [85] Zhonghao Wang, Mo Yu, Yunchao Wei, Rogerio Feris, Jinjun Xiong, Wen-Mei Hwu, Thomas S. Huang, and Honghui Shi. Differential Treatment for Stuff and Things: A Simple Unsupervised Domain Adaptation Method for Semantic Segmentation. In *Proc. of CVPR*, pages 12635–12644, 2020. [5](#)
- [86] Enze Xie, Wenhai Wang, Zhiding Yu, Anima Anandkumar, Jose M. Alvarez, and Ping Luo. SegFormer: Simple and Efficient Design for Semantic Segmentation with Transformers. In *Proc. of NeurIPS*, pages 12077–12090, 2021. [2](#), [6](#), [7](#), [8](#)
- [87] Zhenda Xie, Zheng Zhang, Yue Cao, Yutong Lin, Jianmin Bao, Zhuliang Yao, Qi Dai, and Han Hu. Simmim: A simple framework for masked image modeling. In *Proc. of CVPR*, pages 9653–9663, 2022. [2](#), [4](#)
- [88] Qi Xu, Liang Yao, Zhengkai Jiang, Guannan Jiang, Wenqing Chu, Wenhui Han, Wei Zhang, Chengjie Wang, and Ying Tai. DIRM: Domain-Invariant Representation Learning for Generalizable Semantic Segmentation. In *Proc. of AAAI*, pages 2884–2892, 2022. [2](#)
- [89] Yutaro Yamada and Mayu Otani. Does robustness on image-net transfer to downstream tasks? In *Proc. of CVPR*, pages 9215–9224, 2022. [2](#)
- [90] Fisher Yu, Haofeng Chen, Xin Wang, Wenqi Xian, Yingying Chen, Fangchen Liu, Vashisht Madhavan, and Trevor Darrell. Bdd100k: A diverse driving dataset for heterogeneous multitask learning. In *Proc. of CVPR*, pages 2636–2645, 2020. [5](#), [4](#)
- [91] Qihang Yu, Ju He, Xueqing Deng, Xiaohui Shen, and Liang-Chieh Chen. Convolutions die hard: Open-vocabulary segmentation with single frozen convolutional clip. In *Proc. of NeurIPS*, 2023. [3](#)
- [92] Xiangyu Yue, Yang Zhang, Sicheng Zhao, Alberto Sangiovanni-Vincentelli, Kurt Keutzer, and Boqing Gong. Domain Randomization and Pyramid Consistency: Simulation-to-Real Generalization Without Accessing Target Domain Data. In *Proc. of ICCV*, pages 2100–2110, 2019. [2](#), [4](#)
- [93] Xiangyu Yue, Yang Zhang, Sicheng Zhao, Alberto Sangiovanni-Vincentelli, Kurt Keutzer, and Boqing Gong. Domain randomization and pyramid consistency: Simulation-to-real generalization without accessing target domain data. In *Proc. of ICCV*, pages 2100–2110, 2019. [5](#)
- [94] Yan Zeng, Xinsong Zhang, Hang Li, Jiawei Wang, Jipeng Zhang, and Wangchunshu Zhou. X2-vlm: All-in-one pre-trained model for vision-language tasks. *arXiv preprint arXiv:2211.12402*, 2022. [3](#)
- [95] Jingyi Zhang, Jiaying Huang, Sheng Jin, and Shijian Lu. Vision-language models for vision tasks: A survey. *arXiv preprint arXiv:2304.00685*, 2023. [2](#)
- [96] Kai Zhang, Yifan Sun, Rui Wang, Haichang Li, and Xiaohui Hu. Multiple fusion adaptation: A strong framework for unsupervised semantic segmentation adaptation. *arXiv preprint arXiv:2112.00295*, 2021. [1](#)
- [97] Pan Zhang, Bo Zhang, Ting Zhang, Dong Chen, Yong Wang, and Fang Wen. Prototypical Pseudo Label Denoising and Target Structure Learning for Domain Adaptive Semantic Segmentation. In *Proc. of CVPR*, pages 12414–12424, 2021. [1](#)
- [98] Yuyang Zhao, Zhun Zhong, Na Zhao, Nicu Sebe, and Gim Hee Lee. Style-Hallucinated Dual Consistency Learning for Domain Generalized Semantic Segmentation. In *Proc. of ECCV*, pages 535–552, 2022. [2](#)
- [99] Yiwu Zhong, Jianwei Yang, Pengchuan Zhang, Chunyuan Li, Noel Codella, Liunian Harold Li, Luowei Zhou, Xiyang Dai, Lu Yuan, Yin Li, et al. Regionclip: Region-based language-image pretraining. In *Proc. of CVPR*, pages 16793–16803, 2022. [3](#)
- [100] Zhun Zhong, Yuyang Zhao, Gim Hee Lee, and Nicu Sebe. Adversarial Style Augmentation for Domain Generalized Urban-Scene Segmentation. In *Proc. of NeurIPS*, pages 338–350, 2022. [2](#)
- [101] Bolei Zhou, Hang Zhao, Xavier Puig, Sanja Fidler, Adela Barriuso, and Antonio Torralba. Scene Parsing through ADE20K Dataset. In *Proc. of CVPR*, pages 633–641, 2017. [3](#)
- [102] Jinghao Zhou, Chen Wei, Huiyu Wang, Wei Shen, Cihang Xie, Alan Yuille, and Tao Kong. ibot: Image bert pre-training with online tokenizer. *arXiv preprint arXiv:2111.07832*, 2021. [2](#), [4](#)
- [103] Kaiyang Zhou, Jingkang Yang, Chen Change Loy, and Ziwei Liu. Conditional prompt learning for vision-language models. In *Proc. of CVPR*, pages 16795–16804, 2022. [3](#)
- [104] Kaiyang Zhou, Jingkang Yang, Chen Change Loy, and Ziwei Liu. Learning to prompt for vision-language models. In *IJCV*, 130(9):2337–2348, 2022. [5](#)
- [105] Ziqin Zhou, Yinjie Lei, Bowen Zhang, Lingqiao Liu, and Yifan Liu. Zegclip: Towards adapting clip for zero-shot semantic segmentation. In *Proc. of CVPR*. [3](#)
- [106] Barret Zoph, Golnaz Ghiasi, Tsung-Yi Lin, Yin Cui, Hanxiao Liu, Ekin Dogus Cubuk, and Quoc Le. Rethinking pre-training and self-training. In *Proc. of NeurIPS*, 33:3833–3845, 2020. [2](#)

# VLTseg: Simple Transfer of CLIP-Based Vision-Language Representations for Domain Generalized Semantic Segmentation

## Supplementary Material

### A. ResNet-101 Experiments

In Tab. 6, the domain generalization performance of our VLTseg approach is shown with a ResNet-101 backbone. We observe that also for this setting, VLTseg-R provides SOTA performance. When training on GTA5, we outperform the previous SOTA by +1.2% in the DG mean. It has to be considered that the EVA-02 [74] pre-trained initialization was not available for the ResNet-101 backbone, so the CLIP [59] initialization was used. On Cityscapes and Mapillary, VLTseg-R obtains an even larger margin with +3.2% mIoU and +3.4% mIoU over the previous SOTA, respectively.

When training on Synthia, our VLTseg-R approach also performs competitively with other SOTA methods. However, the performance is slightly lower than FSDR [35] and WEDGE [39], for which, in particular, the performance on BDD100k is higher. That is reasonable because both mentioned approaches utilize external real data during training, which is a clear distinction from our method. That significantly simplifies domain generalization on the challenging Synthia dataset. RICA [75] as the current SOTA on Synthia employs a much more complex framework for domain generalization, including a FeatureGAN for feature-space augmentation. Nevertheless, our VLTseg outperforms this approach on Mapillary.

### B. Loss Ablation

We weighed the loss in all our experiments with  $\lambda_{PTM} = 1$ . We did not conduct hyperparameter tuning and selection because an optimization towards unseen domain is not possible in practice under the domain generalization setting. However, we show the PTM loss behavior for scientific purposes with different weights across our target datasets for training on GTA5 in Fig. 4. The study demonstrates that specific values work better for specific datasets, but overall only in a very few cases larger generalization decreases of  $\sim 4\%$  mIoU on a single dataset can be observed.

### C. Decoder Architecture

We also examine the impact of different decoder architectures on the domain generalization performance, as shown in Tab. 7. The DG mean of the model with the Mask2Former [11] decoder is 1.9% higher than the next best model with Semantic FPN as originally used by DenseCLIP [60] and even 3.1% better than the ASPP-based decoder from DAFormer [29]. VLTseg with a Mask2Former

Table 6. **Domain generalization performance** (mIoU (%)) in comparison with state-of-the-art approaches. Training was performed on the synthetic GTA5 ( $\mathcal{D}^S = \mathcal{D}_{\text{train}}^{\text{GTA5}}$ ) and SYNTHIA ( $\mathcal{D}^S = \mathcal{D}_{\text{train}}^{\text{SYNTHIA}}$ ) datasets. Evaluation is performed on three real-world validation sets ( $\mathcal{D}^T = \mathcal{D}_{\text{val}}$ ). All our experiments employed a CLIP [59] pre-trained ResNet-101 [24] backbone (therefore denoted as VLTseg-R) with a Mask2Former [11] head. Prior work results are cited from the respective paper, only the values for works marked with  $\circ$  are taken from [56].

	DG Method	mIoU (%) on			
		$\mathcal{D}_{\text{val}}^{\text{CS}}$	$\mathcal{D}_{\text{val}}^{\text{BDD}}$	$\mathcal{D}_{\text{val}}^{\text{MV}}$	DG mean
$\mathcal{D}^S$ : GTA5	Baseline [86]	36.1	36.6	43.8	38.8
	IBN-Net $^\circ$ [53]	37.7	36.7	36.8	37.1
	RobustNet $^\circ$ [12]	37.3	38.7	38.1	38.0
	DRPC [92]	42.5	38.7	38.1	39.8
	SW [54]	36.1	36.6	32.6	35.1
	FSDR [34]	44.8	41.2	43.4	43.1
	SAN+SAW [56]	45.3	41.2	40.8	42.4
	WEDGE [39]	45.2	41.1	48.1	44.8
	GTR [55]	43.7	39.6	39.1	40.8
	SHADE [98]	46.7	43.7	45.5	45.3
	WildNet $^\circ$ [45]	45.8	41.7	47.1	44.9
	TLDR [40]	47.6	44.9	48.8	47.1
	RICA [75]	48.0	<b>45.2</b>	46.3	46.5
	VLTseg-R (Ours)	<b>51.2</b>	43.4	<b>52.2</b>	<b>48.3</b>
$\mathcal{D}^S$ : SYNTHIA	Baseline [86]	34.3	27.8	38.0	33.4
	IBN-Net $^\circ$ [53]	34.2	32.6	36.2	34.3
	DRPC [92]	37.6	34.4	34.1	35.4
	SW [54]	36.1	36.6	32.6	35.1
	FSDR [34]	40.8	37.4	39.6	39.3
	SAN+SAW [56]	40.9	36.0	37.3	38.1
	WEDGE [39]	40.9	<b>38.1</b>	<b>43.1</b>	40.7
	GTR [55]	39.7	35.3	36.4	37.1
	RICA [75]	<b>45.0</b>	36.3	41.6	<b>41.0</b>
	TLDR [40]	42.6	35.5	37.5	38.5
	VLTseg-R (Ours)	42.2	31.0	42.5	38.6

[11] decoder performs consistently better across all four real-world datasets than the other decoder architectures. That implies that Mask2Former can leverage the provided

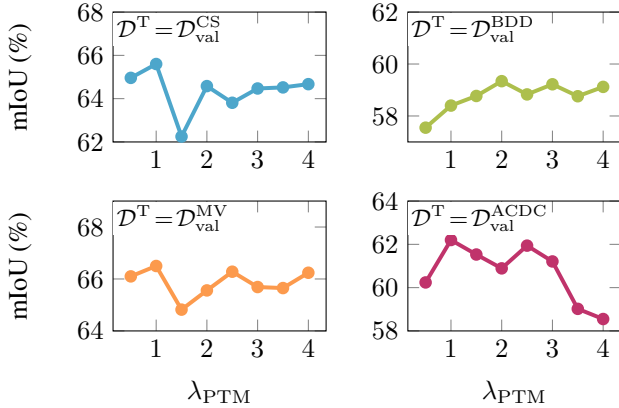


Figure 4. **Ablation study of different  $\lambda_{\text{PTM}}$  loss weights** (mIoU (%)) and their domain generalization performance. Training was performed on the synthetic GTA5 ( $\mathcal{D}^S = \mathcal{D}_{\text{train}}^{\text{GTA5}}$ ) dataset; evaluation on the four shown real-world datasets.

Table 7. **Ablation study of different decoder architectures** and their domain generalization performance (mIoU (%)). Training was performed on the synthetic GTA5 ( $\mathcal{D}^S = \mathcal{D}_{\text{train}}^{\text{GTA5}}$ ) dataset. Evaluation is performed on the four shown real-world datasets.

Decoder	mIoU in %				
	$\mathcal{D}_{\text{val}}^{\text{CS}}$	$\mathcal{D}_{\text{val}}^{\text{BDD}}$	$\mathcal{D}_{\text{val}}^{\text{MV}}$	$\mathcal{D}_{\text{val}}^{\text{ACDC}}$	DG Mean
Semantic FPN [48]	61.6	59.5	65.4	58.8	61.3
Segformer [86]	62.4	58.4	65.3	58.5	61.2
ASPP (DAFormer) [29]	60.8	57.6	63.4	58.7	60.1
Mask2Former [11]	<b>65.6</b>	<b>58.4</b>	<b>66.5</b>	<b>62.2</b>	<b>63.2</b>

language-vision embeddings more effectively and better focus on domain-invariant features.

## D. Real-to-real Ablation

We also conducted an ablation study for the  $\mathcal{L}_{\text{PTM}}$  loss under the real-to-real generalization setting and results are shown in Tab. 8.

We observe that the language guidance during downstream segmentation training is slightly beneficial for most of the datasets and increases in- and out-of domain generalization performance.

## E. Qualitative Results

### E.1. Spatial UMAP

Similar to Dinov2 [52], we also spatially visualize the embeddings of the encoder on a single-image basis to better understand the advantages of vision-language pre-trained initializations. The results are shown in Fig. 5. It be-

Table 8. **Real-to-real domain generalization performance w/ and w/o downstream language guidance by the  $\mathcal{L}_{\text{PTM}}$  loss** (mIoU (%)). Training was performed on the different real-world dataset as shown row-wise. In- and out-of-domain performance evaluation is performed on various real-world validation sets. The in-domain performance is marked with gray. The EVA-02-B-16 encoder was employed and crop size was set to  $512 \times 512$  for this ablation.

	$\mathcal{L}_{\text{PTM}}$	Evaluated on				DG mean	
		$\mathcal{D}_{\text{val}}^{\text{CS}}$	$\mathcal{D}_{\text{val}}^{\text{BDD}}$	$\mathcal{D}_{\text{val}}^{\text{MV}}$	$\mathcal{D}_{\text{val}}^{\text{ACDC}}$		
Trained on	$\mathcal{D}_{\text{train}}^{\text{CS}}$	✗	76.7	57.2	66.1	63.3	65.8
		✓	77.4	57.4	66.6	62.2	65.9
	$\mathcal{D}_{\text{train}}^{\text{BDD}}$	✗	64.7	64.5	64.6	57.8	62.9
		✓	63.6	64.2	65.1	56.6	62.4
	$\mathcal{D}_{\text{train}}^{\text{MV}}$	✗	69.6	62.0	73.7	66.0	67.8
		✓	72.5	61.9	73.6	66.0	68.5
	$\mathcal{D}_{\text{train}}^{\text{ACDC}}$	✗	68.6	56.6	63.2	73.8	65.6
		✓	68.9	56.0	63.8	74.4	65.8

comes visible that an ImageNet supervised pre-trained ViT encoder has similar embeddings for semantically different classes of an unseen domain like Cityscapes. In contrast, vision-language pre-trained initializations from EVA-CLIP [74] have very fine-grained, clearly distinguishable embeddings for different objects in the image. Even within the same object, e.g. the child buggy, different semantic parts have different embeddings.

### E.2. Cityscapes

We show predictions on the Cityscapes test set  $\mathcal{D}_{\text{test}}^{\text{CS}}$  in Fig. 6 which visualizes the high segmentation quality of our VLTseg approach when training supervised on Cityscapes.

### E.3. ACDC

We show predictions on the ACDC test set  $\mathcal{D}_{\text{test}}^{\text{ACDC}}$  in Fig. 7. Even though our model has never seen this domain before during training we can observe that it provides high-quality segmentation maps across challenging adverse weather conditions.

## F. Implementation Details

### F.1. Training settings

We provide an extensive list of our hyperparameters and detailed settings in Tab. 9 to make our experiments reproducible.

For the Mask2Former [11] decoder we used the default settings as provided by the authors.

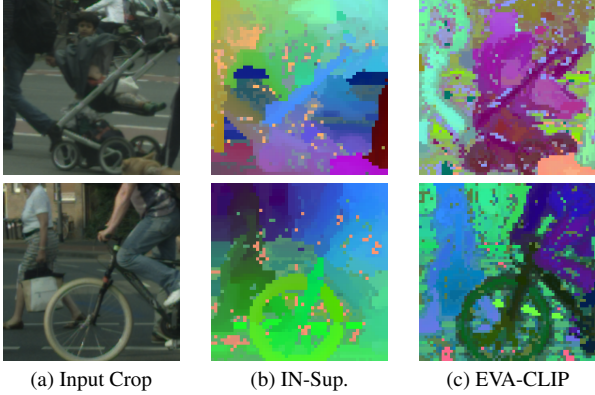


Figure 5. **Image-level UMAP [49] projection of last encoder layer output features to 3 dimensions.** In (b) features of an ImageNet-21k supervised pre-trained ViT (IN-Sup.) encoder are shown. (c) in comparison shows the features of an encoder trained with EVA-CLIP [74] on Laion-2B. The three dimensions are visualized as R, G, and B color intensities. Similar color indicates similar features. The UMAP projections were computed image-wise on Cityscapes [15] validation crops. Features learned by EVA-CLIP show a superior distinction between objects of different semantics, e.g., for the child buggy and also between bicycles and pedestrians.

Table 9. **Experimental Settings**

Hyperparameter		Synthetic-to-Real	Real-to-Real
crop size		512	1024
stride size		426	768
iterations		5k	20k
batch size		16	8
Optimizer	type	AdamW	
	default lr	1e-04	
	backbone lr	1e-05	
	weight_decay	0.05	
	eps	1e-08	
	betas	(0.9, 0.999)	
LR Schedule	type	PolyLR	
	eta_min	0	
	power	0.9	
	begin	500	
Text	context length	13	
	embedding size	768	
	transformer heads	12	
	transformer width	768	
	transformer layers	12	
	Encoder	in_channels	3
patch size		14	
embedding size		1024	
depth		24	
indices		[9, 14, 19, 23]	
output_dim		768	
Decoder		in_channels	[1024, 1024, 1024 + 19, 1024]
	stride	[4, 8, 16, 32]	
	feat_channels	256	
	out_channels	256	
	num_classes	19	
	num_queries	100	
	num_transformer_feat_level	3	
	positional_encoding	128	

Table 10. **Computational complexity of the vision encoders** that were employed in our experiments. GFLOPS and Parameters are computed using MMPreTrain [14], numbers are rounded to integers.

Encoder	Parameters	GFLOPS
ViT-B-16	87	88
ViT-L-16	304	311
SAM-L-16	308	397
EVA-02-S-16	22	32
EVA-02-B-16	86	107
EVA-02-L-14	303	508

For the ablation with the PTM loss and the EVA-02-S-16 model we interpolated the text encoder output projection in bilinear mode to match the vision encoder output shape of 384. In addition the vision encoder was initialized from MIM training and the text encoder from EVA-02-B-16 CLIP.

## F.2. Test set evaluation

For the evaluation on the Cityscapes [15] and ACDC [65] test set we followed the corresponding common practice.

For Cityscapes test set evaluation, we first trained our VLT-Seg model on Mapillary for 20k iterations as also done by previous state-of-the-art approaches [4, 5, 84]. Afterwards, 40k fine-tuning iterations on the official  $\mathcal{D}_{\text{train}}^{\text{CS}}$  dataset with 2975 images were conducted. In contrast to the other works, no additional data like the coarse annotations were used. Both trainings used  $1024 \times 1024$  resolution. We used multi-scale evaluation with [1.0, 1.25, 1.5, 1.75, 2.0, 2.25] image ratios and random flip as test-time augmentation during inference. Test set evaluation was done on the full  $2048 \times 1024$  resolution.

For the ACDC test set evaluation, we trained for 20k iterations on  $1024 \times 1024$  crops only on Cityscapes  $\mathcal{D}_{\text{train}}^{\text{CS}}$  without using any ACDC data. The test set inference was similar to Cityscapes with a multi-scale evaluation with [1.0, 1.25, 1.5, 1.75] image ratios and on the full  $1920 \times 1080$  resolution.

## G. Computational complexity of vision encoders

We show the GFLOPS and parameters of the vision encoders employed in our experiments in Tab. 10. We used three variants of the ViT with base, large, and SAM and a patch size of 16. Moreover, we employed three complexities of EVA: small, base, and large. Due to the architectural modifications, EVA has more GFLOPS than ViT at a similar number of parameters.



Figure 6. Predictions on Cityscapes test set  $\mathcal{D}_{\text{test}}^{\text{CS}}$ . Training and evaluation was conducted as described in Appendix F.2

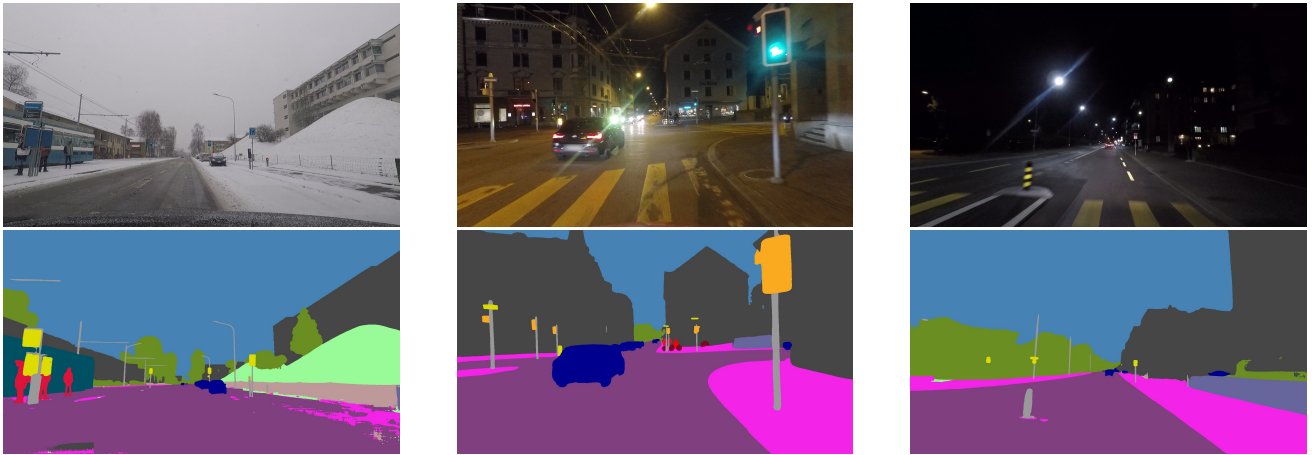
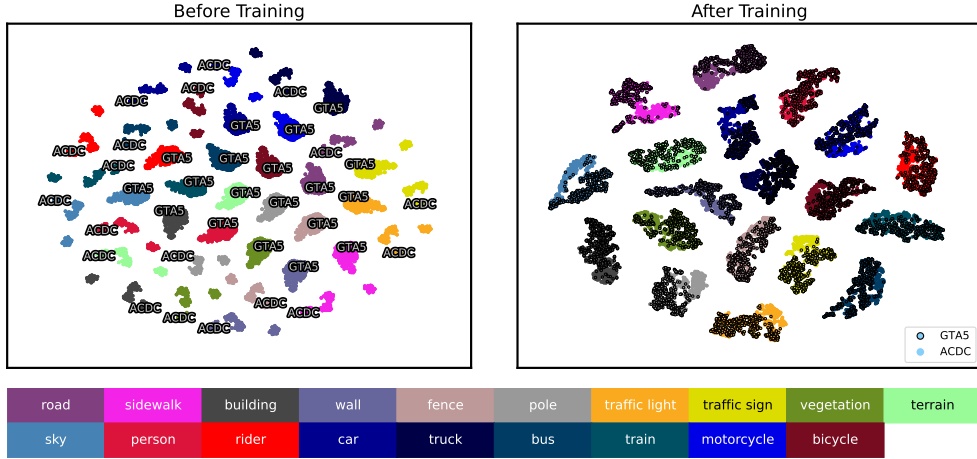


Figure 7. Predictions on the ACDC test set  $\mathcal{D}_{\text{test}}^{\text{ACDC}}$ . Training and evaluation was conducted as described in Appendix F.2

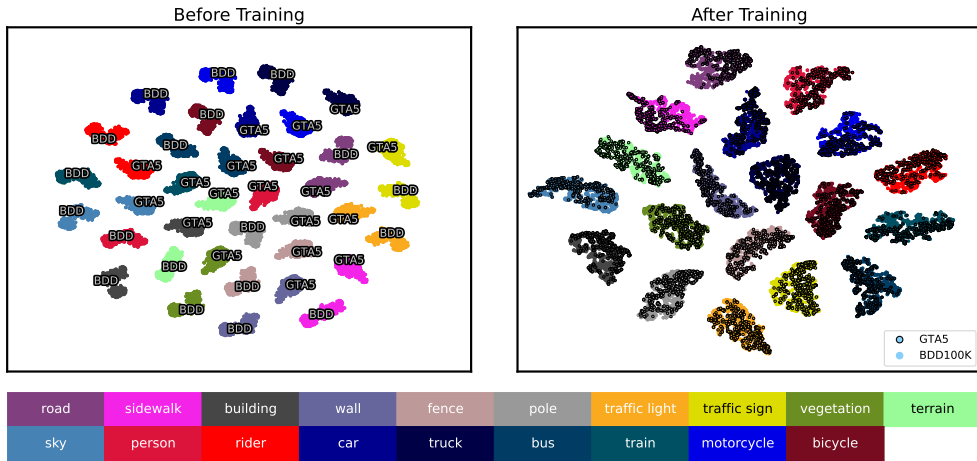
## H. Feature Space Analysis

Similar to the feature space analysis in the main part, we conducted the same analysis for the other real-world datasets ACDC [65], BDD100k [90] and Mapillary [51] in comparison with the embeddings from the synthetic GTA5 [61] dataset. The results are shown in Fig. 8.

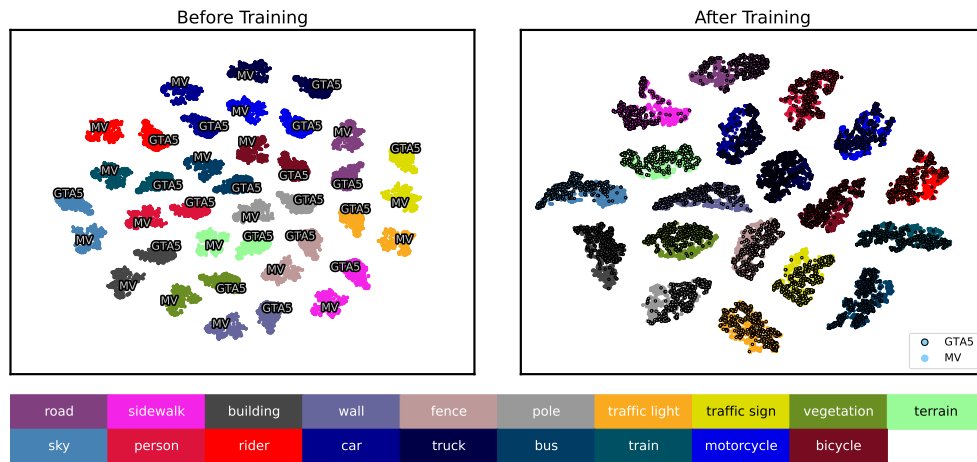
We observe that the synthetic and real-world embeddings are well-aligned for all three real-world target datasets after the synthetic source-only training even though the network has never seen any of the real-world images before. All the corresponding classes show a significant overlap which can, however, slightly vary among the datasets and classes. The class traffic light for instance shows a better overlap for BDD100k and Mapillary but slightly worse for ACDC.



GTA → ACDC



GTA → BDD100k



GTA → Mapillary

Figure 8. t-SNE feature space analysis between GTA5 and three real-world datasets Mapillary, ACDC and BDD100k. We sampled 500 images from  $\mathcal{D}_{\text{train}}^{\text{GTA5}}$  and the real-world validation sets  $\mathcal{D}_{\text{val}}^{\text{MV}}$ ,  $\mathcal{D}_{\text{val}}^{\text{ACDC}}$  and  $\mathcal{D}_{\text{val}}^{\text{BDD}}$  and extracted the embeddings of our best performing VLTseg network after the text encoder, where both language and vision features are fused. In the plots after training, the GTA5 embeddings are denoted with black circles around their data points. From the plots, we can see that synthetic source and real target class clusters are well aligned and overlap after our VLTseg training. Best viewed digitally.